Electrokinetic trapping and surface enhanced Raman scattering detection of biomolecules using optofluidic device integrated with a microneedles array

Yu-Luen Deng[1] and Yi-Je Juang[1,2,3,a)]
[1]*Department of Chemical Engineering, National Cheng Kung University, No. 1 University Road, Tainan 70101, Taiwan*
[2]*Center for Micro/Nano Science and Technology, National Cheng Kung University, No. 1 University Road, Tainan 70101, Taiwan*
[3]*Research Center for Energy Technology and Strategy, National Cheng Kung University, No. 1 University Road, Tainan 70101, Taiwan*

(Received 28 November 2012; accepted 7 February 2013; published online 21 February 2013)

In this study, microneedles which possess sharp tips were utilized to trap and detect the biomolecules. Owing to the large curvature, the tips of the microneedles created a substantially high gradient of electric field under the non-uniform electric field which served as not only the trapping sites but also the substrate for surface enhanced Raman scattering (SERS). Separation of polystyrene microparticles with different sizes and two kinds of biomolecules (*Staphylococcus aureus* (*S. aureus*) and the red blood cells (RBCs)) were demonstrated. Moreover, *in situ* detection of *S. aureus* was performed immediately after separation was completed. The results showed that, after 15 s of sample collection, the Raman signals of *S. aureus* were detected and greatly enhanced through SERS effect. © *2013 American Institute of Physics*. [http://dx.doi.org/10.1063/1.4793224]

I. INTRODUCTION

In recent years, the development of optofluidics has led to the realization of various applications such as bio-sensing, optical source, particle transport, displays, imaging, and many review articles can be found in the literature.[1–6] Optofluidics involves integration of microfluidics and optics at the same platform where fluid and light are driven to interact.[4] One well-established category of optofluidics is the device consisting of homogeneous liquids with varying refractive indices. This can be utilized to construct the optical switcher, diffusion-controlled splitter, and liquid-liquid lenses when the incident light passes through the smooth liquid-liquid interfaces.[7] Another category is incorporation of suspended particles inside the optofluidic device such that applications of optical components, transporting, sensing, and analyzing particles are realized through particle manipulation. For the latter category, the ability to control the motion and locations of the particles is the key to the success of the optofluidic device. Different forces have been utilized to manipulate the particles such as mechanical, electrical, optical, thermal, and magnetic forces.[1] Among them, dielectrophoresis (DEP) is one of the most popular methods owing to its label-free nature, favorable scaling effects, simplicity of the instrumentation, and ability to induce both positive and negative forces.[8] DEP is the particle motion occurred in non-uniform AC electric field and commonly applied to manipulate microscopic particles in microfluidic devices. As mentioned previously, there are two types of DEP motion which are induced by non-uniform electric field.[9] When the particles are more polarized than the medium, they move to the region with the highest electric field gradient (e.g., the edge of the electrodes) and this is called positive DEP (pDEP). On the other hand, when the particles

a)Author to whom correspondence should be addressed. Electronic mail: yjjuang@mail.ncku.edu.tw. Tel.: +886 62757575 ext. 62653. Fax: +886 62344496.

are less polarized than the medium, they move to the region with the lowest electric field gradient (e.g., the center of the electrodes or between electrodes), and this is called negative DEP (nDEP).[10–17] For a spherical neutral particle, the time-averaged DEP force is given by

$$F_{DEP} = 2\pi a^3 \varepsilon_m \mathrm{Re}(f_{CM}) \nabla |E|^2, \quad (1)$$

where a is radius of the particle, ε_m is the permittivity of the medium, $\nabla|E|^2$ is the gradient of the square of the applied electric field strength, and $\mathrm{Re}(f_{CM})$ is the real partition of the complex Clausius–Mossotti (CM) factor. The CM factor is given by the following:

$$f_{CM} = (\varepsilon_p^* - \varepsilon_m^*)/(\varepsilon_p^* + 2\varepsilon_m^*), \quad (2)$$

where $\varepsilon^* = \varepsilon - i(\sigma/2\pi\omega)$ is the complex permittivity, and the subscripts p and m stand for particle and medium, respectively. σ is conductivity, ω is the frequency of the applied alternating current, and $I = \sqrt{-1}$. The value of $\mathrm{Re}(f_{CM})$ ranges from -0.5 to 1. The particle experiences pDEP force when $\mathrm{Re}(f_{CM})$ is greater than zero and nDEP when $\mathrm{Re}(f_{CM})$ is less than zero. At some frequency, $\mathrm{Re}(f_{CM})$ becomes zero, that is, the particle does not experience any DEP force and the operating frequency is called the crossover frequency. Note that, for the particle having multi-shell structure, it may not be able to predict the particle motion under the non-uniform electric field since there might be more than one crossover frequency and the $\mathrm{Re}(f_{CM})$ becomes too complicated to be evaluated.

DEP as the driving force to manipulate bio-particles has been well demonstrated. For example, interdigitated castle electrode was exploited to separate latex beads with different sizes and trap different types of viruses.[17] Applying DEP in conjunction with fluid flow allows one to separate dead and live yeast cells in the microfluidic device.[18] The dielectrophoretically responsive label was used to discriminate labeled *E. coli* from those without being labeled in the DEP-activated cell sorting device.[19] The pathogen was separated and collected at the roughened Au surface for subsequent SERS detection.[20] Separation of mouse melanoma clones with different melanin contents by DEP was also demonstrated.[21]

In recent years, surface-enhanced Raman spectroscopy (SERS) has been utilized to detect biomolecules such as cells, bacteria, viruses, and DNAs.[22–25] SERS effect was first observed on the roughened silver electrode with pyridine monolayer[26] and has been investigated for decades.[27–31] It originates from the surface plasmon resonance (SPR) which is the result of interaction between nano-scaled metallic structure and the excitation laser. Although, there are two proposed mechanisms for SERS (one is chemical enhancement and the other is electromagnetic enhancement[27–30,32–34]), it is believed that the magnitude of enhancement on SERS mainly results from electromagnetic effect.[33–36] SERS can be realized by two strategies. One is called homogeneous SERS, which is performed by using metallic nanoparticles as the Raman enhancer.[35,37] The other is called heterogeneous SERS, for which the target in solution interacts with patterned metallic structure on the substrate.[20,23,37–40] When detecting low concentration of analytes, the heterogeneous SERS method is usually adopted owing to its better sensitivity. However, diffusion of analytes to the SERS active site is time-consuming and fabrication of substrate with uniform SERS effect is relatively complicated. To resolve these issues, various strategies have been exploited such as applying dielectrophoresis (DEP) to collect biomolecules at the roughened gold surface,[20] utilizing the junction between micro- and nano- channels to concentrate protein and perform SERS detection.[40]

In this paper, we fabricated a microfluidic device integrated with silicon sharp tips, which is capable of carrying out sample separation, concentration, and SERS detection simultaneously. It has been shown that there is strong enhancement of electromagnetic fields at the sharp features and the regions with large curvature.[32] This is referred to tip enhanced Raman spectroscopy (TERS)[41–46] effect. Meanwhile, the microneedles array electrode can provide extremely high gradient of electric field to generate greater DEP force, which benefits sample concentration in a relatively short time. The effect of SERS and separation, concentration and detection of biomolecules are presented.

II. EXPERIMENTAL

A. Device fabrication

Figure 1 shows the schematic and photo of the DEP microfluidic device. A 6 in. (1,0,0) silicon wafer was cleaned by standard RCA clean protocol, followed by deposition of 2 μm thick SiO_2 layer on the silicon substrate inside the PECVD system (Plasma Lab system 100, Oxford). After patterning by the photolithographic process, SiO_2 was etched (BOE, HF:NH_4F = 1:6) to form an array of circles with 80 μm in diameter and 150 μm in center-to-center distance. The silicon chip then went through cryogenic etching. The gas streams of O_2 and SF_6 were supplied and mixed in the chamber at the ratio of 1:10 and the RF power was set to 1 W. The etching rate was maintained at 2.2 μm/min. The fabricated microneedles array was then deposited with Au/Ti (200 nm/30 nm) conductive layer by using electron beam evaporator. The deposition rate of Au/Ti layer was set to 0.1 Å/s.

For the opposite electrode in the DEP device, the ITO glass was used. The microchannel was constructed by cutting the PET double sided adhesive tape with 70 μm in thickness by CO_2 laser machine and placing it between the ITO glass and the microneedles array electrode to bond them together.

B. Sample preparation

The latex beads with 0.92 μm and 4.8 μm diameters were purchased from Thermo scientific. The original stock solution containing 1% (w/v) solid was diluted to the concentration of 10^8 beads/ml in DI water. Gram positive bacteria, *Staphylococcus aureus* (*S. aureus*, BCRC 14957) were cultured on tryptic soy agar (TSA) at 35 °C. The bacteria were labeled by mixing with a FITC-SPA labeling kit on a vortex machine at room temperature for 1 h, followed by being centrifuged and washed twice by PBS buffer and re-suspended into 1 ml PBS buffer with 10^8 CFU (colony-forming units per milliliter)/ml. There are two reasons for only labeling *S. aureus*. One is that the size of *S. aureus* is much smaller than that of RBC, which will make it difficult to observe *S. aureus* without fluorescence labeling. The other is that it will be hard to distinguish *S. aureus* from RBC if both biomolecules are labeled with a fluorescence kit. Rhodamine 6 G powder was purchased from Sigma-Aldrich and 10^{-5}M aqueous solution was prepared.

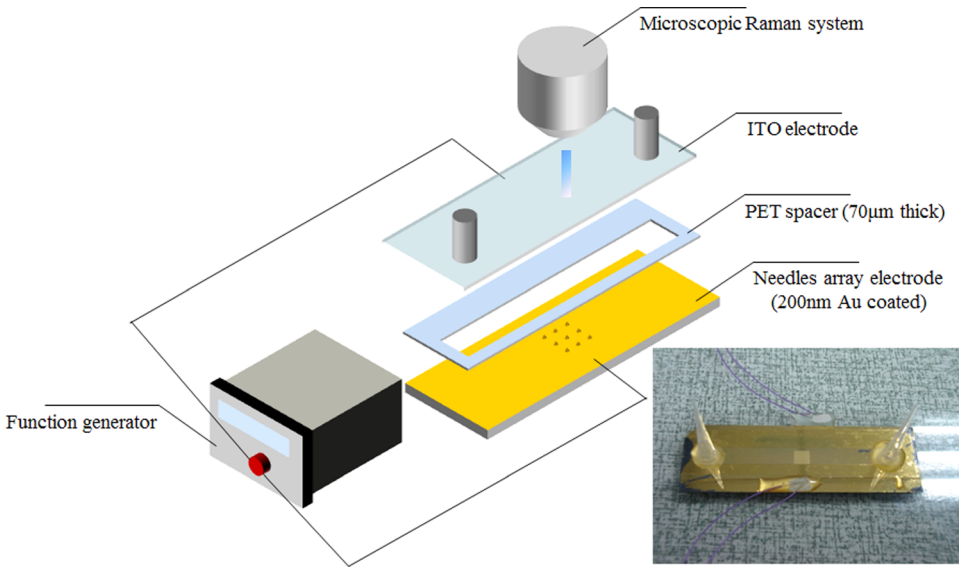

FIG. 1. Schematic and photo of DEP microfluidic device.

C. DEP separation of latex beads with different sizes

The solution containing latex beads with different sizes were loaded into the DEP device. To determine the crossover frequency of the latex beads, the frequency sweep was performed, where the AC power with 10 Vp-p was set and frequency was tuned from 10 MHz to 1 kHz. The movement of particles was observed by inverted fluorescence microscope (Nikon, TE2000-S) and recorded by CCD (Photometrics, Cool Snap HQ2) for analysis. To minimize adhesion of particles to the electrode, the microchannel was purged with 1 ml of 3%(w/v) BSA aqueous solution at a flow rate of 0.5 μl/min, followed by 1 ml DI water at flow rate of 1 μl/min prior to loading the particle solution.

D. DEP separation of *S. aureus*/RBCs

Since only the *S. aureus* were labeled with the fluorescence kit, the visible light was turned on to observe RBCs. From the literature, the crossover frequencies of *S. aureus* and RBCs were found around 6 MHz and 700 kHz at 1.3 mS/cm of medium conductivity,[20] respectively. To collect *S. aureus* at the tips by pDEP and repel RBCs away from the needle by nDEP, the operating frequency needs to be between the crossover frequencies of *S. aureus* and RBCs and the crossover frequency of *S. aureus* should be lower than that of RBCs. To obtain the proper crossover frequencies for these two biomolecules, 1X phosphate buffered saline (PBS buffer) diluted by 300 mM sucrose at the ratio of 1:270 was used to adjust the conductivity of the medium to 80 μS/cm and maintain the identical osmotic pressure in RBCs. The crossover frequencies of *S. aureus* and RBCs were then determined to be around 100 kHz and 250 kHz, respectively. DEP separation of *S. aureus*/RBCs was carried out at 170 kHz and 10 Vp-p.

E. Raman detection of R6G and *S. aureus* using a microneedles array

To demonstrate the SERS effect, 10 μl R6G solution with 10^{-5} M was dispensed on an Au coated microneedles array, followed by 15 min of drying. SERS measurement was then conducted by using a confocal microscopic Raman spectrometer (Renishaw, United Kingdom) after the substrate was rinsed by DI water several times. A HeNe laser at 633 nm was used as the excitation source. The laser power was set at 1 mW and scattering signals were collected by 10X objective lens which was connected to Raman detector. The Raman shift was calibrated at 520 cm^{-1}, the signal peak generated from cleaned silicon wafer. The exposure time and accumulation times were set 10 s and 1 time, respectively. The range of Raman shift was set from 50 cm^{-1} to 3500 cm^{-1} and the background fluorescence caused by glass substrate was corrected by WIRE 3.2 software. Raman detection of *S. aureus* was carried out 2 min after turning on AC. To prevent *S. aureus* from damage, the exposure time was decreased from 10 s to 1 s and accumulation times were increased from 1 to 2 times.

III. RESULTS AND DISCUSSION

A. SEM images of a silicon microneedles array

Figure 2(a) shows SEM images of the etched microneedles. In the etching process, the ratio of O_2 and SF_6 is critical since they are used to produce a SiO_xF_y passivation layer on silicon substrate.[47–50] When the flow rate of O_2 increases, the anisotropic etching prevails because of greater protection from thick SiO_xF_y passivation layer and the microstructures with vertical sidewall are obtained. On the other hand, the isotropic etching effect dominates when O_2 flow rate decreases. In this study, isotropic etching was achieved, and the microneedles have the aspect ratio around 0.5. In addition, it can be seen that microneedles were over etched near the edge at the large area (2 * 2 cm^2), where the height and the sharpness of the needles were apparently less than those at the center of array. More uniform and sharp microneedles were obtained when a smaller patterned area (0.5 * 0.5 cm^2) was used. The tip size of most of the needles was less than 200 nm. It was reported that, for the larger patterned area, the distance from the center to the edge is larger, which may poses difficulty in removing the reaction byproduct from the center of array.[51] This leads to

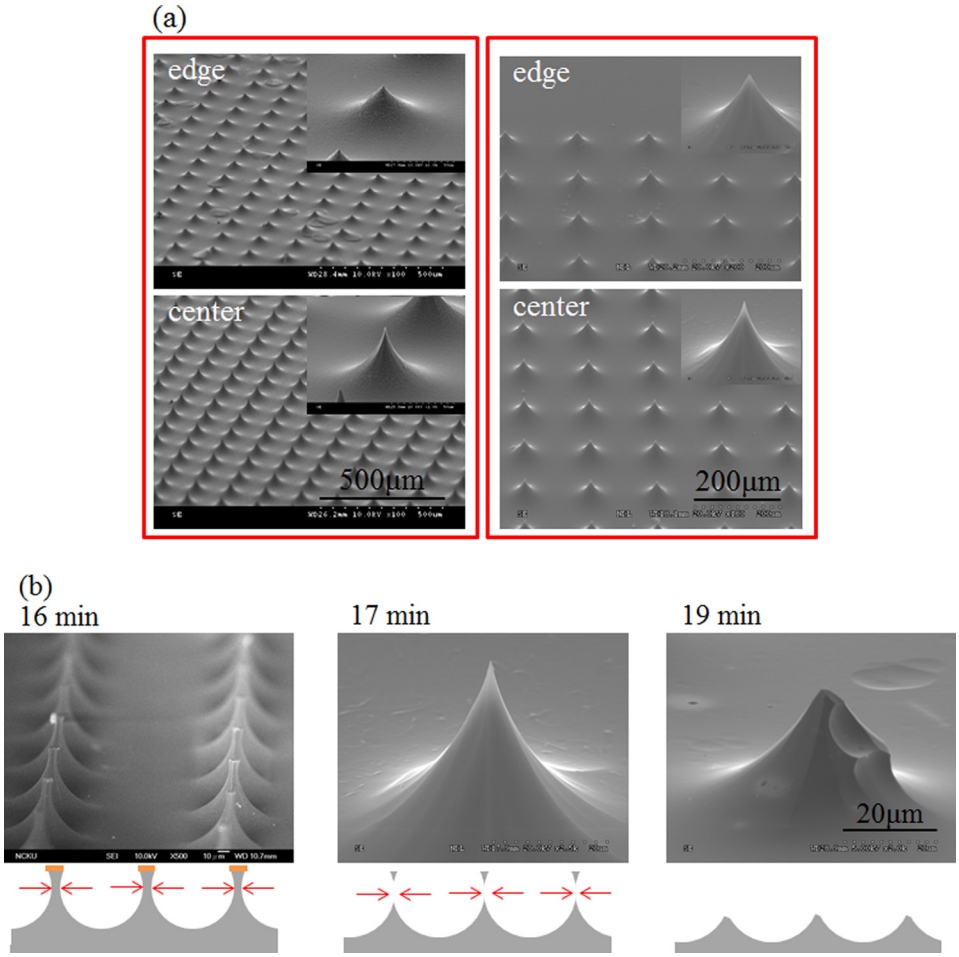

FIG. 2. (a) The effect of patterned area on etching uniformity. Left: large patterned area (2 * 2 cm^2). Right: small patterned area (0.5 * 0.5 cm^2). (b) Time-lapsed images of microneedles fabricated during the etching process.

the higher etching rate at the edge of the array than that at the center. Figure 2(b) shows the time-lapse images of microneedles array in the etching process. The hourglass-like structure was formed at the etching time around 16 min. When the etching time increased to 17 min, the "neck" of hourglass-like structure was trimmed and broke, resulting in formation of the microneedles with sharp tips. Further increase of etching time leads to over etching of the microneedles.

B. DEP separation of latex beads with different sizes

The crossover frequency of the latex beads can be evaluated by the following equation:[52]

$$\omega_{CO} = (3/2\pi^2)(D/a^2)(E_s\lambda F/RT)^2,$$

where $E_s\lambda$ is the Zeta potential of the latex beads in DI water, D is the diffusivity of the beads in DI water, a is the diameter of the bead, T is the temperature, F is the Faraday's constant, and R is the ideal gas constant. From the literature, $E_s\lambda$ is found to be around 200 mV.[53] D is approximately 1.4 * 10^{-7} m^2/s. At the room temperature, the crossover frequencies of 0.92 μm and 4.8 μm latex beads in DI water are estimated to be around 1 MHz and 40 kHz, respectively. The experimental measurement of the crossover frequencies for 0.92 μm and 4.8 μm particles in DI water were around 2 MHz and 10 kHz, respectively, which is in the right range of the estimation. Figure 3 shows the time-lapse images of DEP separation of latex beads with different sizes. The dashed circles indicate the region surrounding the tips of the microneedles.

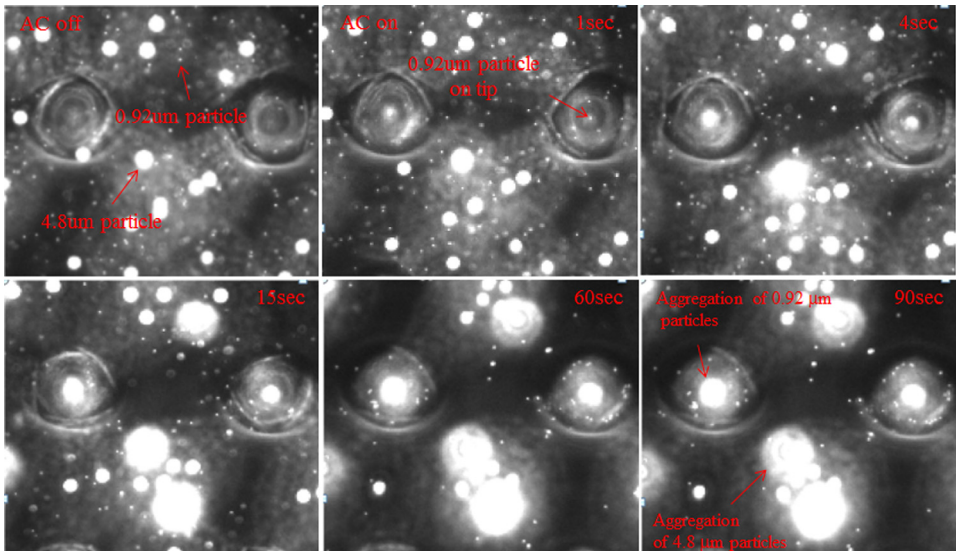

FIG. 3. Time-lapsed images of DEP separation of latex beads with different sizes. The dashed circles indicate the region surrounding the tips of microneedles.

Before turning on AC, the microparticles were randomly distributed in the solution. After turning on AC, the 0.92 μm particles started moving toward the tips of microneedles, while 4.8 μm particles were repelled from the tips. Since the operating frequency was 100 kHz, the 0.92 μm particles would experience pDEP, while the 4.8 μm particles nDEP according to their crossover frequencies. After 15 s, most of the 0.92 μm particles aggregated at the tips of microneedles, while the 4.8 μm particles at the area between four microneedles.

C. Raman detection of R6G at the tips

Figure 4 shows the Raman spectra obtained by using a gold coated silicon wafer with and without a microneedles array. When using the gold coated substrate without a microneedles

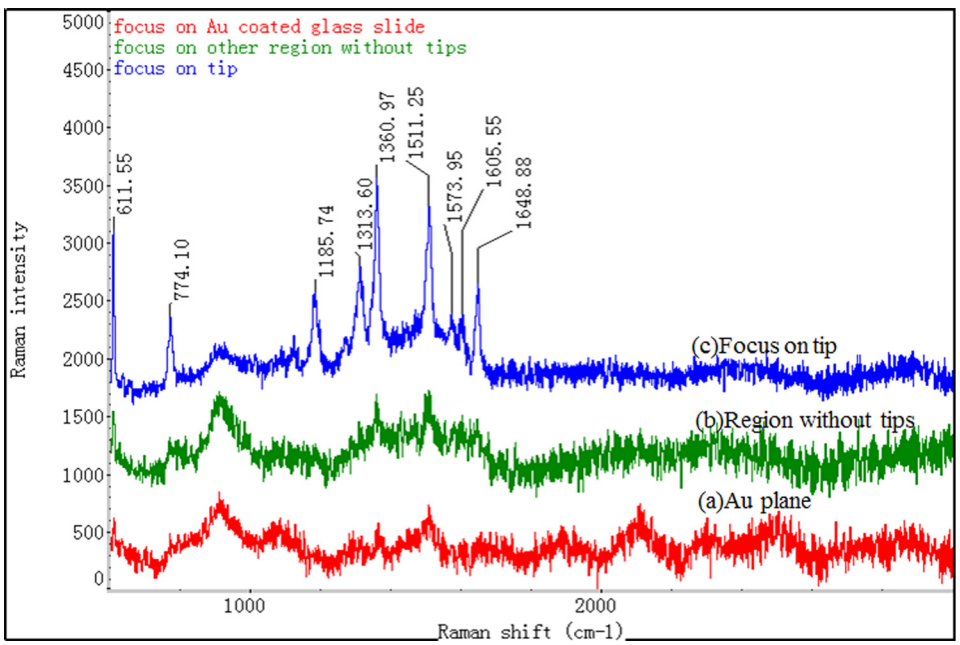

FIG. 4. Raman detection of R6G molecules on the gold coated substrate and substrate with microneedles array.

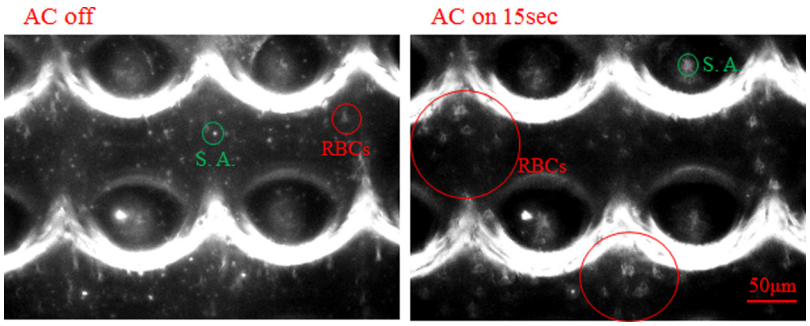

FIG. 5. Time-lapsed images of DEP separation of *S. aureus* and RBCs.

array, it can be seen that only three clear signals of R6G molecules (620 cm^{-1}, 1342 cm^{-1}, and 1515 cm^{-1}) were detected. When switching to the gold coated substrate with a microneedles array and focusing the laser beam on the tips, not only the intensity of these three peaks increased, but six more peaks (780 cm^{-1}, 1195 cm^{-1}, 1300 cm^{-1}, 1562 cm^{-1}, 1585 cm^{-1}, 1659 cm^{-1}) were detected as well. Note that, when the laser beam was focused on the area away from the tips, the spectra and intensity of the signals were similar to those obtained at gold coated plane. This indicates that sharp tips indeed provide enhancement of Raman signals.

D. On-chip separation of *S. aureus*/RBCs and SERS analysis of *S. aureus*

Figure 5 shows the time-lapse images of *S. aureus* and RBCs inside the DEP optofluidic microdevice before and after AC was turned on. Before AC was turned on, *S. aureus* and RBCs were randomly distributed inside the microdevice. The smaller bright dots are *S. aureus* while the larger, irregular shaped dots are RBCs. After turning on AC at the 170 kHz operating frequency for 15 s, *S. aureus* experienced pDEP and moved toward the tips of microneedles to form aggregation as shown in Figure 5. Meanwhile, RBCs experienced nDEP and were repelled from the tips. *In situ* Raman detection of *S. aureus* was performed and the Raman spectra are shown in Figure 6. There are two clear peaks (1160 cm^{-1} and 1518 cm^{-1}) with five more peaks

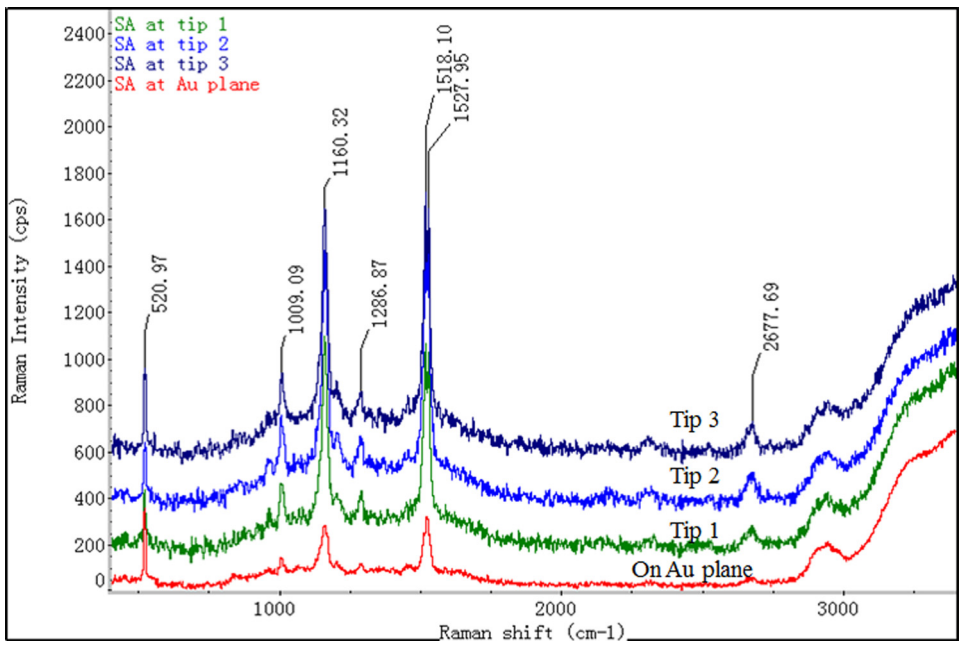

FIG. 6. SERS spectra of *S. aureus* acquired from the gold coated substrate and substrate with microneedles array.

(1009, 1203, 1286, 2304, and 2677 cm^{-1}). Compared to the Raman spectra obtained by using gold coated plane, the Raman signals were enhanced approximately 6 folds, which is comparable to others' work when detecting *S. aureus* via the heterogeneous SERS approach.[20] Note that the signal at 520 cm^{-1} of Raman shift was detected which could be due to the defect of gold deposition. To examine the SERS effect across the chip, the laser beam was focused on the tips of three randomly selected microneedles. It can be seen that the Raman spectra nearly overlapped with each other, indicating uniform SERS effect across the chip.

IV. CONCLUSION

In this paper, we have constructed and demonstrated a DEP optofluidic microdevice for sample separation, concentration and *in situ* SERS detection. The sharp tips of the microneedles not only serve as the DEP trapping sites but also provide SERS effect for detection. The etching process was optimized to acquire better uniformity of microneedles with sharp tips. Using the DEP optofluidic device as fabricated, *S. aureus* with a concentration of 10^8 CFU/ml was detected and analyzed within 30 s.

[1]A. A. Kayani, K. Khoshmanesh, S. A. Ward, A. Mitchell, and K. Kalantar-Zadeh, Biomicrofluidics **6**(3) 031501 (2012).
[2]S. K. Lee, S. H. Kim, J. H. Kang, S. G. Park, W. J. Jung, G. R. Yi, and S. M. Yang, Microfluid. Nanofluid. **4**(1–2), 129–144 (2008).
[3]U. Levy and R. Shamai, Microfluid. Nanofluid. **4**(1–2), 97–105 (2008).
[4]C. Monat, P. Domachuk, C. Grillet, M. Collins, B. J. Eggleton, M. Cronin-Golomb, S. Mutzenich, T. Mahmud, G. Rosengarten, and A. Mitchell, Microfluid. Nanofluid. **4**(1–2), 81–95 (2008).
[5]D. Psaltis, S. R. Quake, and C. H. Yang, Nature **442**(7101), 381–386 (2006).
[6]C. Monat, P. Domachuk, and B. J. Eggleton, Nat. Photonics **1**(2), 106–114 (2007).
[7]Y. Fainman, *Optofluidics: Fundamentals, Devices and Applications* (McGraw-Hill, New York, 2010).
[8]B. Cetin and D. Q. Li, Electrophoresis **32**(18), 2410–2427 (2011).
[9]H. A. Pohl, K. Pollock, and J. S. Crane, J. Biol. Phys. Chem. **6**(3–4), 133–160 (1978).
[10]N. G. Green and H. Morgan, J. Phys. D **30**(11), L41–L44 (1997).
[11]N. G. Green and H. Morgan, J. Phys. D **30**(18), 2626–2633 (1997).
[12]N. G. Green, H. Morgan, and J. J. Milner, J. Biochem. Biophys. Methods **35**(2), 89–102 (1997).
[13]H. Morgan and N. G. Green, J. Electrost. **42**(3), 279–293 (1997).
[14]H. Morgan, N. G. Green, M. P. Hughes, W. Monaghan, and T. C. Tan, J. Micromech. Microeng. **7**(2), 65–70 (1997).
[15]N. G. Green and H. Morgan, J. Phys. D **31**(7), L25–L30 (1998).
[16]A. Ramos, H. Morgan, N. G. Green, and A. Castellanos, J. Phys. D **31**(18), 2338–2353 (1998).
[17]H. Morgan, M. P. Hughes, and N. G. Green, Biophys. J. **77**(1), 516–525 (1999).
[18]I. Doh and Y. H. Cho, Sens. Actuators, A **121**(1), 59–65 (2005).
[19]X. Y. Hu, P. H. Bessette, J. R. Qian, C. D. Meinhart, P. S. Daugherty, and H. T. Soh, Proc. Natl. Acad. Sci. U.S.A. **102**(44), 15757–15761 (2005).
[20]I. F. Cheng, C. C. Lin, D. Y. Lin, and H. Chang, Biomicrofluidics **4**(3), 034104 (2010).
[21]A. C. Sabuncu, J. A. Liu, S. J. Beebe, and A. Beskok, Biomicrofluidics **4**(2), 021101 (2010).
[22]J. Kneipp, H. Kneipp, W. L. Rice, and K. Kneipp, Anal. Chem. **77**(8), 2381–2385 (2005).
[23]T. Park, S. Lee, G. H. Seong, J. Choo, E. K. Lee, Y. S. Kim, W. H. Ji, S. Y. Hwang, and D. G. Gweon, Lab Chip **5**(4), 437–442 (2005).
[24]J. H. Jung, J. Choo, D. J. Kim, and S. Lee, Bull. Korean Chem. Soc. **27**(2), 277–280 (2006).
[25]J. Kneipp, H. Kneipp, M. McLaughlin, D. Brown, and K. Kneipp, Nano Lett. **6**(10), 2225–2231 (2006).
[26]M. Fleischm, P. J. Hendra, and Aj. McQuilla, Chem. Phys. Lett. **26**(2), 163–166 (1974).
[27]D. L. Jeanmaire and R. P. Vanduyne, J. Electroanal. Chem. **84**(1), 1–20 (1977).
[28]K. Kneipp, Y. Wang, H. Kneipp, I. Itzkan, R. R. Dasari, and M. S. Feld, Phys. Rev. Lett. **76**(14), 2444–2447 (1996).
[29]K. Kneipp, Y. Wang, H. Kneipp, L. T. Perelman, I. Itzkan, R. Dasari, and M. S. Feld, Phys. Rev. Lett. **78**(9), 1667–1670 (1997).
[30]K. Kneipp, H. Kneipp, G. Deinum, I. Itzkan, R. R. Dasari, and M. S. Feld, Appl. Spectrosc. **52**(2), 175–178 (1998).
[31]K. Kneipp, H. Kneipp, V. B. Kartha, R. Manoharan, G. Deinum, I. Itzkan, R. R. Dasari, and M. S. Feld, Phys. Rev. E **57**(6), R6281–R6284 (1998).
[32]M. Moskovits, Rev. Mod. Phys. **57**(3), 783–826 (1985).
[33]K. Kneipp, H. Kneipp, R. Manoharan, I. Itzkan, R. R. Dasari, and M. S. Feld, J. Raman Spectrosc. **29**(8), 743–747 (1998).
[34]K. Kneipp, H. Kneipp, I. Itzkan, R. R. Dasari, and M. S. Feld, Chem. Rev. **99**(10), 2957 (1999).
[35]H. Kneipp and K. Kneipp, J. Raman Spectrosc. **36**(6-7), 551–554 (2005).
[36]K. Kneipp, H. Kneipp, and J. Kneipp, Acc. Chem. Res. **39**(7), 443–450 (2006).
[37]Y. S. Huh, A. J. Chung, B. Cordovez, and D. Erickson, Lab Chip **9**(3), 433–439 (2009).
[38]J. Jung, L. X. Chen, S. Lee, S. Kim, G. H. Seong, J. Choo, E. K. Lee, and C. H. Oh, Anal. Bioanal. Chem. **387**(8), 2609–2615 (2007).
[39]S. Lee, J. Choi, L. Chen, B. Park, J. B. Kyong, G. H. Seong, J. Choo, Y. Lee, K. H. Shin, E. K. Lee, S. W. Joo, and K. H. Lee, Anal. Chim. Acta **590**(2), 139–144 (2007).
[40]H. S. Cho, B. Lee, G. L. Liu, A. Agarwal, and L. P. Lee, Lab Chip **9**(23), 3360–3363 (2009).

[41]E. J. Zeman and G. C. Schatz, J. Phys. Chem. **91**(3), 634–643 (1987).
[42]A. Otto, I. Mrozek, H. Grabhorn, and W. Akemann, J. Phys.: Condens. Matter **4**(5), 1143–1212 (1992).
[43]N. Hayazawa, T. Yano, H. Watanabe, Y. Inouye, and S. Kawata, Chem. Phys. Lett. **376**(1–2), 174–180 (2003).
[44]T. Ichimura, N. Hayazawa, M. Hashimoto, Y. Inouye, and S. Kawata, Phys. Rev. Lett. **92**(22), 220801 (2004).
[45]P. Verma, K. Yamada, H. Watanabe, Y. Inouye, and S. Kawata, Phys. Rev. B **73**(4), 045416 (2006).
[46]P. Verma, T. Ichimura, T. Yano, Y. Saito, and S. Kawata, Laser Photon. Rev. **4**(4), 548–561 (2010).
[47]S. Henry, D. V. McAllister, M. G. Allen, and M. R. Prausnitz, J. Pharm. Sci. **87**(8), 922–925 (1998).
[48]H. Jansen, M. de Boer, H. Wensink, B. Kloeck, and M. Elwenspoek, Microelectron. J. **32**(9), 769–777 (2001).
[49]G. Marcos, A. Rhallabi, and P. Ranson, J. Vac. Sci. Technol. B **22**(4), 1912–1922 (2004).
[50]M. J. de Boer, J. G. E. Gardeniers, H. V. Jansen, E. Smulders, M. J. Gilde, G. Roelofs, J. N. Sasserath, and M. Elwenspoek, J. Microelectromech. Syst. **11**(4), 385–401 (2002).
[51]C. Hedlund, H. O. Blom, and S. Berg, J. Vac. Sci. Technol. A **12**(4), 1962–1965 (1994).
[52]S. Basuray, H. H. Wei, and H. C. Chang, Biomicrofluidics **4**(2) 022801 (2010).
[53]M. Sureda, A. Miller, and F. J. Diez, Electrophoresis **33**(17), 2759–2768 (2012).